BSGF - Earth Sciences Bulletin 2019, 190, 4
© A. Pochon *et al.*, Published by EDP Sciences 2019
https://doi.org/10.1051/bsgf/2019004

BSGF
Earth Sciences Bulletin
Available online at:
www.bsgf.fr

A Sb ± Au mineralizing peak at 360 Ma in the Variscan belt

Anthony Pochon[1,2,*], Yannick Branquet[1,3], Eric Gloaguen[2,3], Gilles Ruffet[1], Marc Poujol[1], Philippe Boulvais[1], Charles Gumiaux[3], Florence Cagnard[2], Jean-Marc Baele[4], Inoussa Kéré[1] and Denis Gapais[1]

[1] Université Rennes, CNRS, Géosciences Rennes – UMR 6118, 35000 Rennes, France
[2] BRGM, 45060 Orléans, France
[3] ISTO, UMR 7327, Université d'Orléans, CNRS, BRGM, 45071 Orléans, France
[4] Géologie Fondamentale et Appliquée, Université de Mons, Rue de Houdain 9, 7000 Mons, Belgium

Received: 28 May 2018 / Accepted: 16 February 2019

Abstract – $^{40}Ar/^{39}Ar$ absolute dating on tobelite (an ammonium-rich white mica) has been performed in order to provide geochronological constraints on the Sb ± Au mineralization and hydrothermalism at the Saint-Aubin-des-Châteaux base metal-Sb ± Au occurrence (Variscan Central Armorican Domain, France). The results show that the Sb ± Au deposition occurred at *ca.* 360 Ma. Coupled with recent results obtained in neighboring areas, this occurrence seems to belong to a large-scale Early Carboniferous economic Sb ± Au mineralizing peak in the southeastern part of the Central Armorican Domain. The emplacement of a coeval widespread mafic magmatism in the region appears to represent a major trigger for this mineralizing system at shallow depths (less than 3 km). In the light of these new data, this Early Carboniferous mafic magmatic event must be considered for the overall understanding of the genesis of mineralizing systems at the scale of the whole Variscan belt. Finally, at Saint-Aubin-des-Châteaux, evidence of an Early Permian hydrothermal event is also reported through LA-ICP-MS U-Pb dating of fluorapatite, arguing for the re-use and re-opening of Early Carboniferous mineralizing plumbing system by late (*i.e.* Permian) fluid flow pulses although no metal mobilization was associated with this event.

Keywords: Sb ± Au mineralization / Armorican Massif / $^{40}Ar/^{39}Ar$ dating / tobelite

Résumé – Un pic minéralisateur à Sb ± Au à 360 Ma au sein de la chaîne varique. La datation sur tobelite (mica blanc riche en ammonium) par la méthode $^{40}Ar/^{39}Ar$ a été effectuée afin de fournir des contraintes géochronologiques sur la minéralisation Sb ± Au et l'hydrothermalisme associé à l'occurrence polymétallique de Saint-Aubin-des-Châteaux (Domaine Centre Armoricain, France). Les résultats montrent que les métaux Sb et Au se sont déposés aux alentours de 360 Ma. Couplés avec les résultats récemment obtenus au sein de zones voisines, cette occurrence semble appartenir à un pic de grande échelle, minéralisateur et économique en Sb ± Au dans la partie sud-est du Domaine Centre Armoricain. La mise en place synchrone d'un magmatisme mafique relativement répandu dans la région apparaît comme un élément déclencheur, majeur pour ce système minéralisé à faible profondeur (moins de 3 km de profondeur). À la lumière de ces données nouvelles, le magmatisme mafique dévono-carbonifère doit dorénavant être pris en considération pour la compréhension de la genèse des systèmes minéralisés à l'échelle de la chaîne varisque. Enfin, à Saint-Aubin-des-Châteaux, un événement hydrothermal du Permien précoce est également identifié par la datation U-Pb de la fluorapatite par LA-ICP-MS, plaidant pour une réutilisation et une réouverture du système minéralisés dévono-carbonifère par des circulations de fluides tardives (*i.e.* Permien) sans qu'il n'y ait de mobilisation de métaux associés à cet évènement.

Mot clés : minéralisations à Sb ± Au / Massif Armoricain / datation $^{40}Ar/^{39}Ar$ / tobelite

*Corresponding author: pochon.anthony@gmail.com

1 Introduction

Dating hydrothermal events remains a major challenge for geochronologists. This is often linked to the lack of minerals suitable for radiochronological dating within the mineralization paragenetic sequence itself. If such suitable minerals exist, this can also be due to either:

- poorly-constrained paragenetic sequence;
- low parent isotopes contents in these phases (low-uranium content in apatite for example);
- their incapacity to retain sufficient amounts of daughter isotopes (*e.g.* Ar loss in mica).

In addition, overprints due to thermal input and/or successive fluid flow frequently disturb the isotopic system of the chronometers, which might yield meaningless ages (*e.g.* Tartèse *et al.*, 2011, 2015).

For these main reasons and with the exception of U deposits (Ballouard *et al.*, 2017, 2018a), the timing of the Armorican metallic mineralized systems remains poorly constrained. This is particularly true for the Sb ± Au mineralization from the Variscan Central Armorican Domain (CAD, Fig. 1a) that hosts numerous deposits such as the giant La Lucette deposit. In this study, we focus on mineralizing system where Sb is described, either as the dominant economic metal resource or as secondary valuable metal. In addition to Sb, we compiled data from Au ± Sb occurrences because Au and Sb are intimately associated in paragenetic sequences from the Variscan belt (*e.g.* Bouchot *et al.*, 1997, 2005). To date, the timing of Armorican Sb ± Au mineralization is constrained by only a few radiometric ages and mainly by indirect and relative geological relationships (see Fig. 1b for a compilation of the available data and constraints). Sb ± Au mineralization is considered to be Late Variscan in age (*ca.* 310–295 Ma) and associated with major shear zones in the region (Chauris & Marcoux, 1994). Similar chronological constraints have been proposed for the Sb ± Au mineralization of the Variscan Iberian Massif in northern Portugal (Fig. 1b). For the French Massif Central, Bouchot *et al.* (2005) proposed a general unified tectonic-hydrothermal model, the so-called Or 300 Ma event ("Or" stands for gold in French), involving large-scale fluid flow related to thermal event during the post-thickening collapse of the orogen (Costa & Rey, 1995). In such scenario, the mineralizing peak is associated with the coeval emplacement of W ± Sn-rich leucogranites and rare-metal granites (Costa & Rey, 1995; Bouchot *et al.*, 2005; Chauvet *et al.*, 2012). Consequently, the Armorican Sb ± Au occurrences, including those of the CAD (*i.e.* La Lucette or the Le Semnon deposits, Fig. 1a), were associated with this metalliferous peak around 300 Ma (Bouchot *et al.*, 1997).

However, several lines of evidence argue against such model for the Sb ± Au mineralization in the CAD. Indeed, the CAD represents the external domain of the orogen and did not experience significant thickening (*i.e.* no metamorphic nappe stacking, see Gumiaux *et al.*, 2004 and references therein). Furthermore, there is no evidence for late to post-orogenic extension in the CAD, in contrast to the South Armorican domain (SAD). Then, subsequent fluid flows driven by thermal effect, as evidenced by granite emplacements or migmatization during post-orogenic collapse, are missing all together and make therefore this Late Carboniferous fluid flows scenario unlikely. Furthermore, recent works by Pochon *et al.* (2016a, b, 2018) highlighted a strong spatial and temporal relationship between a widespread mafic magmatism at *ca.* 360 Ma and the Le Semnon Sb ± Au mineralization (Figs. 1a and 1b). Indeed, the Le Semnon Sb ± Au deposit was formed before 340 Ma with an unequivocal contribution of a 360–350 Ma event revealed by $^{40}Ar/^{39}Ar$ and U-Pb ages on hydrothermal illite and apatite, respectively. Although geometry, hydrothermal evolution, alteration processes and the nature of fluids are comparable (Chauris *et al.*, 1985; Chauris & Marcoux, 1994; Bouchot *et al.*, 1997, 2005; Pochon *et al.*, 2018), at least one Sb ± Au deposit was so far identified as older than the Late Variscan orogenic evolution in the CAD.

In this study, we focus on the Saint-Aubin-des-Châteaux Sb ± Au occurrence within the CAD (see location Fig. 1a), because several fluid flows are recorded in this location (Fig. 1b, Tartèse *et al.*, 2015). This occurrence is a famous locality for metallogenists (type locality for oolitic ironstone-hosted gold deposit, Gloaguen *et al.*, 2007, 2016) and mineralogists dealing with rare mineral species (Lulzacite: Léone *et al.*, 2000; Moëlo *et al.*, 2000; Frost *et al.*, 2014; Pretulite: Moëlo *et al.*, 2002; Tobelite: Mesto *et al.*, 2012; Capitani *et al.*, 2016) or hydrothermal phosphates (Sr-Apatite: Moëlo *et al.*, 2008; Xenotime: Tartèse *et al.*, 2015). Therefore, based on these numerous studies, this occurrence presents the advantage to have a well-constrained hydrothermal paragenetic sequence.

We report a new $^{40}Ar/^{39}Ar$ 360 Ma old age on this Sb ± Au hydrothermal system performed on tobelite (an uncommon ammonium-rich white mica, $(NH_4, K)Al_2(Si_3Al)O_{10}(OH)_2$). Then, we discuss the meaning of this age with respect to regional tectonics, magmatism and hydrothermalism. In addition, a new U-Pb data on apatite allow to yield a subordinate Permian late hydrothermal perturbation.

2 Geological background

2.1 Regional geology

Located in the Variscan Armorican belt, the Saint-Aubin-des-Châteaux (SADC) occurrence belongs to the Central Armorican Domain (CAD), which is bounded by two dextral crustal-scale wrench zones (Gumiaux *et al.*, 2004 and references therein): the North Armorican Shear Zone (NASZ) and the South Armorican Shear Zone (SASZ) (Fig. 1a), respectively. The CAD is mostly composed of a Late Neoproterozoic to Cambrian pelitic basement with an Ordovician to Devonian sedimentary cover, both affected by a low greenschist facies metamorphism. During the Carboniferous, the whole CAD underwent a N125°E trending regional-scale dextral simple shearing that produced upright folds with N110°E trending sub-horizontal axes and sub-vertical axial planes (Gapais & Le Corre, 1980; Gumiaux *et al.*, 2004). Large-scale wavelength folds are mechanically controlled by the thickness of the competent Armorican quartzite formation (Fig. 2a) and are associated with a weakly developed sub-vertical N110°E trending cleavage bearing a sub-horizontal stretching lineation (Gapais & Le Corre, 1980; Gumiaux *et al.*, 2004). Strain intensity increases from North to South reaching its maximum near the northern branch of the SASZ (Gapais & Le Corre, 1980). A dominant N160°E trending regional faulting (Figs. 1a and 2a) is compatible with the regional dextral simple shear (Choukroune *et al.*, 1983).

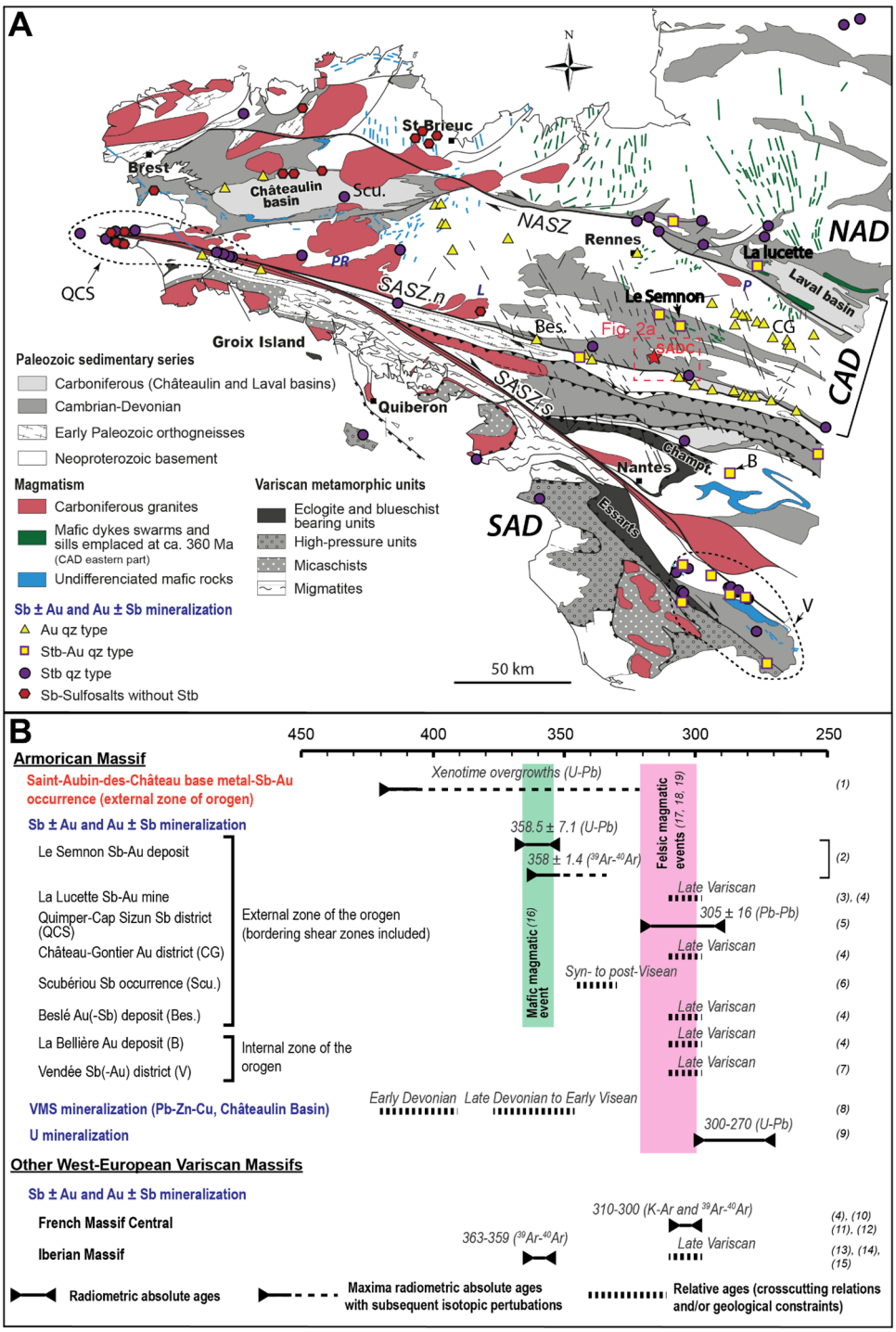

Fig. 1. A. Geological map of the Armorican Massif with location of the different Sb-Au mineralization types. The eastern parts of both the Central Armorican Domain (CAD) and the Cadomian northern domain suffered important basic magmatism attested by numerous dolerite dyke swarms and sills (in green) at *ca.* 360 Ma (Pochon *et al.*, 2016b). A high-density network of kilometre-scale NNW-SSE-trending vertical faults affects the CAD to the south of Rennes city. NASZ: North Armorican Shear Zone; SASZ.n,.s: South Armorican Shear Zone, northern and southern branches respectively; Champt: Champtoceaux metamorphic complex; PR, L, P: Pontivy-Rostrenen, Lizio and Le Pertre granites respectively; SADC: Saint-Aubin-Des-Châteaux (red star). B. Age compilation of Sb-Au mineralized systems through the Western European Variscan orogenic segments. Armorican Base metal VMS and U mineralization have also been reported. The deposits or districts are localized on 1A (name abbreviation). (1) Tartèse *et al.* (2015), (2) Pochon *et al.* (2018), (3) Chauris and Marcoux (1994), (4) Bouchot *et al.* (1997), (5) Marcoux and Fouquet (1980), (6) Pierrot *et al.* (1975), (7) Marcoux *et al.* (1984), (8) Lescuyer *et al.* (1997), (9) Ballouard *et al.* (2018a), (10) Charonnat (2000), (11) Bouchot *et al.* (2005), (12) Chauvet *et al.* (2012), (13) Couto *et al.* (1990), (14) Neiva *et al.* (2008), (15) Hall *et al.* (1997), (16) Pochon *et al.* (2016b), (17) Augier *et al.* (2015), (18) Capdevila (2010), (19) Ballouard *et al.* (2018b).

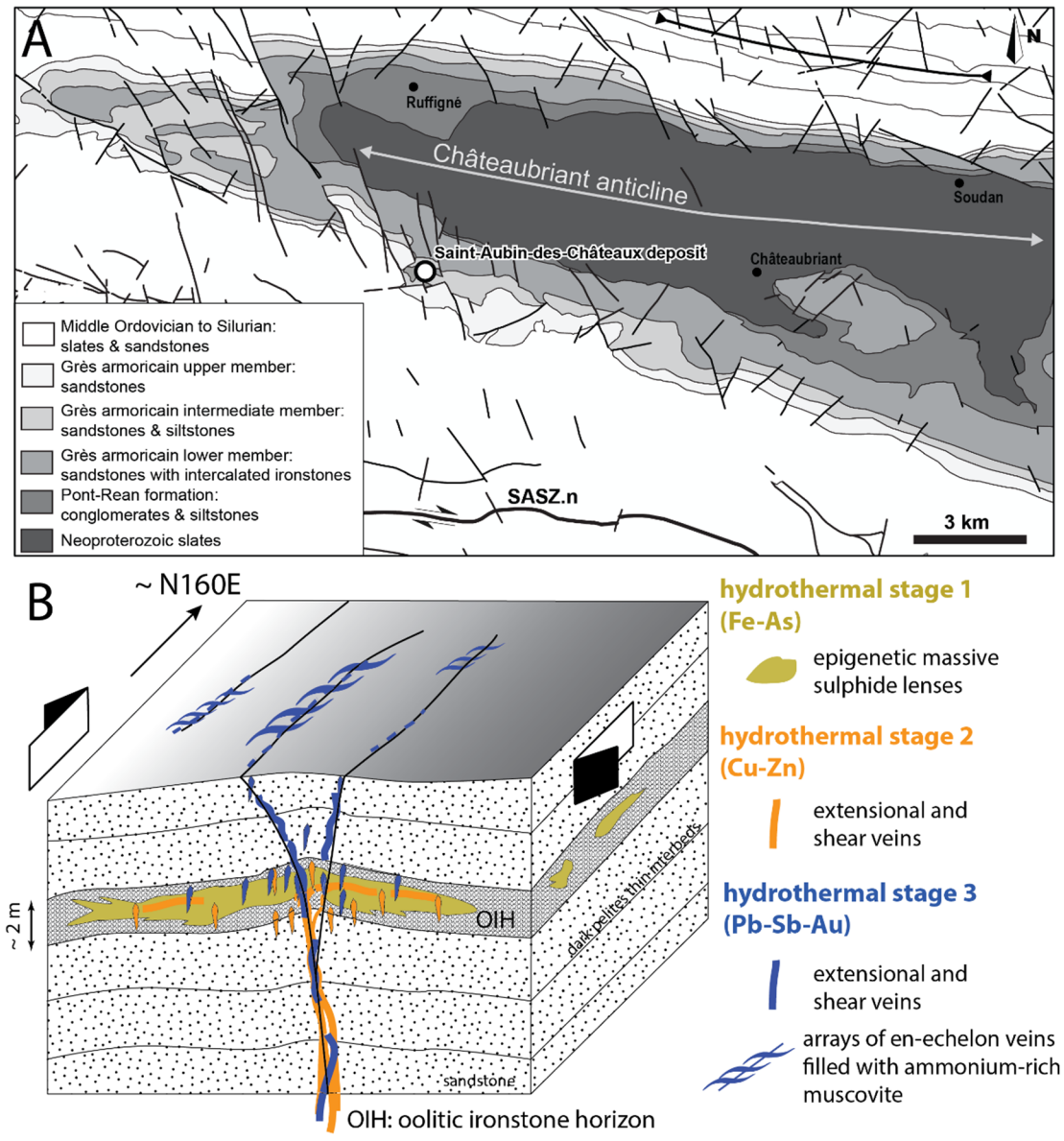

Fig. 2. A. Geological map of the area around the SADC base metal-Sb-Au occurrence located in the very low dipping anticline southern flank. The SADC quarry is located within an important N160-150-E-trending fault corridor. B. Simplified and synthetic structural framework of the SADC mineralizing system. Second-order faults (*e.g.* Riedel shear) are not shown. All stages of hydrothermal fluid flows are channelized by vertical strike-slip faults. Intersection of this fault system with OIH triggered the intense massive sulphidation of this reactive horizon.

Contrary to the western part of the CAD, the eastern part of the region experienced rather limited granitic intrusions. Some synkinematic granite intrusions were emplaced at *ca.* 320–315 Ma along the northern branch of the SASZ, such as the Lizio granite (Tartèse *et al.*, 2011) while an older granitic intrusion occurs near the NASZ, the Le Pertre granite (343 ± 3 Ma by U-Pb on zircon, Vernhet *et al.* (2009), Fig. 1a). On the other hand, the CAD is intruded by a widespread network of mafic dikes and sills (Fig. 1a) linked to a regional magmatic event dated at *ca.* 360 Ma (Pochon *et al.*, 2016b). This magmatic event is therefore coeval with the high-pressure metamorphic event identified in the South Armorican Domain (Bosse *et al.*, 2000, 2005) and with the beginning of the bulk dextral wrenching of the CAD (Gumiaux *et al.*, 2004). As mentioned in the introduction, this mafic magmatic event has strong spatiotemporal and likely genetic relationships with some Sb ± Au deposits from the CAD (Pochon *et al.*, 2016a, 2017, 2018, Fig. 1a). Note that the base metal VMS-type deposits recognized in the Châteaulin Carboniferous Basin (Figs. 1a and 1b), as well as other VMS-type deposits in the French Massif Central (*e.g.* Lescuyer *et al.*, 1997) and the Iberian Pyrite Belt (Yesares *et al.*, 2015 and reference therein) were also formed around ~360 Ma.

2.2 The Saint-Aubin-des-Châteaux base metal-Sb ± Au occurrence

The SADC polymetallic deposit, located on the southern flank of the Châteaubriant anticline (Fig. 2a), is mainly hosted by the lower member of the Armorican Quartzite that consists of homogeneous massive sandstone beds intercalated with cm thick dark pelitic beds. At a regional scale, four main oolitic ironstone horizons (OIH; Fig. 2b) intercalated within the lower part of the Armorican Quartzite have been recognized (Chauvel, 1974). In the SADC deposit, only the uppermost OIH is currently cropping out. OIH were affected by diagenesis and by the regional low-grade metamorphism (Le Corre, 1978), as indicated by the growth of a low-grade Sr-bearing fluorapatite (Moëlo *et al.*, 2008). Early metal free hydrothermal circulations and alterations are recorded in the OIH by several successive growth of hydrothermal xenotime (Tartèse *et al.*, 2015) and early quartz-chlorite veins (Gloaguen *et al.*, 2007). Following early barren fluid circulations, four main successive stages of OIH epigenetic hydrothermal alteration have been distinguished (see Gloaguen *et al.*, 2007 for detailed paragenetic sequence). A strong hydrothermal alteration began with a massive epigenetic sulphidation event evidenced along cross-cutting vertical strike-slip faults (stage 1 Fe-As, Fig. 2b), where the OIH is pervasively replaced by a pyrite-pyrrhotite-arsenopyrite assemblage. The sulphidation front across the OIH front is marked by the growth of hydrothermal apatite and REE-phosphates (Moëlo *et al.*, 2002, 2008). Then, a second base-metal stage is characterized by extensional and shear veins, crosscutting the massive sulphide lenses, and mainly filled with a quartz, pyrite, chalcopyrite, sphalerite and galena assemblage (stage 2, Cu-Zn(-Pb), Fig. 2b). A subsequent Pb-Sb ± Au stage 3 (hereafter named Sb ± Au stage 3), still related to vertical strike-slip faults activity (Fig. 2b), is characterized by veins filled with Sb-sulphosalts and base-metal sulphides (bournonite, boulangerite, tetrahedrite, pyrite, sphalerite, chalcopyrite, galena; Figs. 3a–3c) and associated electrum (Fig. 3b). A maximum temperature of 390–350 °C has been established for stage 1, while stage 2 and 3 took place at temperature of 300 and 275 °C (Gloaguen *et al.*, 2007), respectively. En-echelon veins arrays and polymetallic veins of stage 3 are often filled with peculiar mm to cm-sized ammonium-rich white micas (tobelite and NH_4^+-rich muscovite) (Figs. 2b, Figs. 3a–3f). Tobelite occurrences are controlled by organic matter enclosed in OIH and in dark pelitic thin interbeds, and are therefore associated with antimony and gold deposition. A fourth stage led to carbonate deposition.

The hydrothermal plumbing system of the SADC is fully controlled by right-lateral wrenching accommodated by N160E-trending sub-vertical faults (Fig. 2b) crosscutting a local-scale N120°E-trending anticline. In detail, the kinematic analysis of shear and extensional veins shows that successive increments of non-coaxial dextral shearing are recorded by the different vein orientations and their respective hydrothermal mineral fillings (*i.e.* stage 1, 2 or 3, Gloaguen *et al.*, 2007). Based on the structural analysis and coupled with the regional strain restoration of Gumiaux *et al.* (2004), Gloaguen *et al.* (2007) suggested a long-time span for the SADC hydrothermal system: the massive sulphidation stage 1 might have initiated around 340–330 Ma, while the final Sb ± Au stage 3 formed later around 310–300 Ma, *i.e.* in accord with published relative age constraints for such mineralization elsewhere in the Armorican Massif (*e.g.* Chauris & Marcoux, 1994; Fig. 1b). More recently, based on their REE characteristics, Tartèse *et al.* (2015) dated three generations of xenotime found as epitaxial overgrowths on detrital zircon within the OIH. Their growths are attributed to successive hydrothermal events (Moëlo *et al.*, 2002). U-Pb systematics of xenotime grains were disturbed by these successive events resulting in the scatter of apparent ages between ~420 and ~330 Ma (Fig. 1b). Tartèse *et al.* (2015) interpreted the younger dates cluster around ~340–330 Ma as coeval with stages 1 and 2.

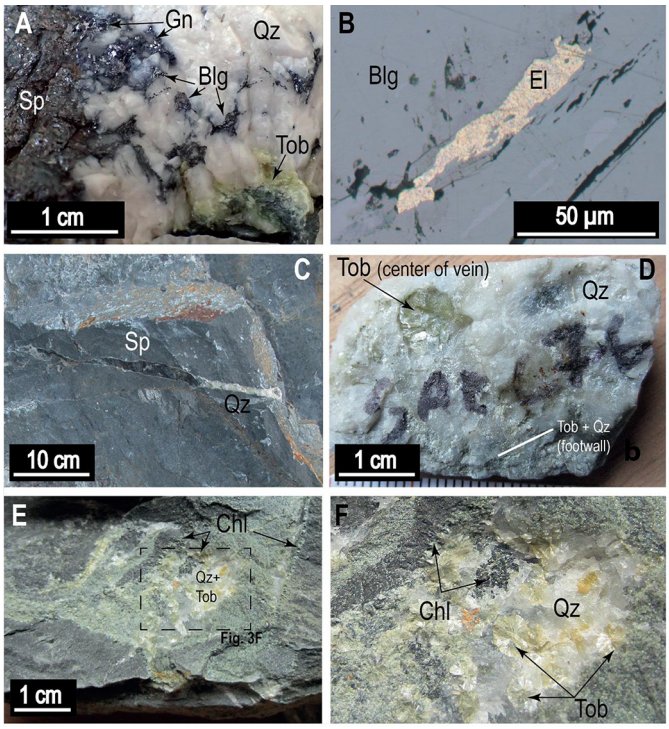

Fig. 3. A. Typical Pb-Sb-Au vein of the stage 3 from SADC. Wall rocks (to the left) are rich in sphalerite (Sp) and galena (Gn) whereas vein centre (to the right) shows sulfosalts (here boulangerite, Blg) and tobelite (Tob) enclosed within a quartz gangue. B. Polished thin section microphotograph (reflected polarized light) of boulangerite (Blg) and electrum (El) of the stage 3 assemblage at SADC. C. Quartz vein with sphalerite in the Armorican quartzite. D. SADC76 sample consists of quartz vein with tobelite crystals. E. Sample rock of Armorican quartzite with veinlets of quartz, chlorite (Chl), tobelite. F. Zoom of mineralogical association of chlorite, tobelite and quartz.

3 Mineralogical characterization of tobelite

Tobelite is a rare mineral species and has never been used for dating of hydrothermal mineralization. It generally occurs as very fine grains (< 1 mm) within sedimentary rocks rich in organic components where NH_4-mica formation is attributed to N liberation during the thermal decomposition of organic matter (Bentabol & Cruz, 2016 and references therein). Nevertheless, black shales-hosted tobelite-bearing quartz veins associated with a hydrothermal gold event have been already

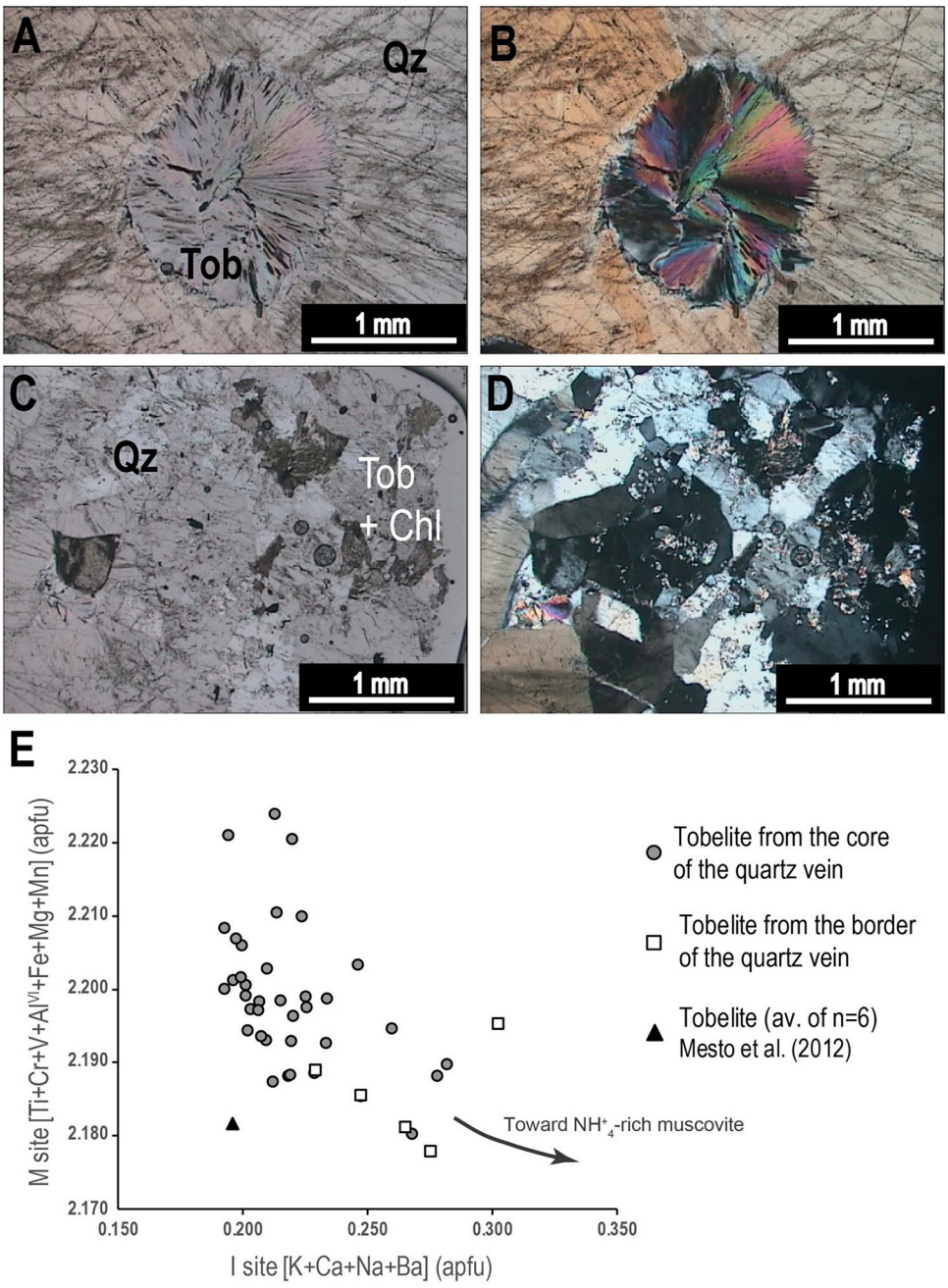

Fig. 4. Tobelite (Tob) crystal in the core of the quartz (Qz) vein from the SADC76 sample (A. in plane-polarized light and B. between crossed polars). Tobelite crystals with Chlorite (Chl) along the vein border from the SADC76 sample (C. in plane-polarized light and D. between crossed polars). E. Plot of M site *vs.* I site of tobelite grains, from the SADC76 sample, analyzed by electron microprobe. In addition to this, the average of tobelite analyses from Mesto *et al.* (2012) is plotted.

described in Utah (Wilson *et al.*, 1992). Tobelite (crystal size ~500 μm) from Utah is associated with kaolinite, quartz, chlorite, Fe-oxides, interstratified illite/smectite and pyrite in quartz veins enriched in Hg, As, Se, T1, Sb, Sc, and Mo (Wilson *et al.*, 1992). At SADC, scarce tobelite may occur as exceptionally large crystals up to 1 cm within epigenetic hydrothermal veins (Figs. 3a, 3d). This rather unusual large size permitted a crystallographic characterization of the tobelite species (Mesto *et al.*, 2012; Capitani *et al.*, 2016). The infill of tobelite-bearing quartz veins (up to 10 cm thick) is heterogeneous. It could be made of sulphides-only or disseminated sulphides and tobelite within quartz associated with a rim of chlorite or tobelite. Then, tobelite occurs as isolated radiating crystal aggregates in quartz (Figs. 3d–3f and

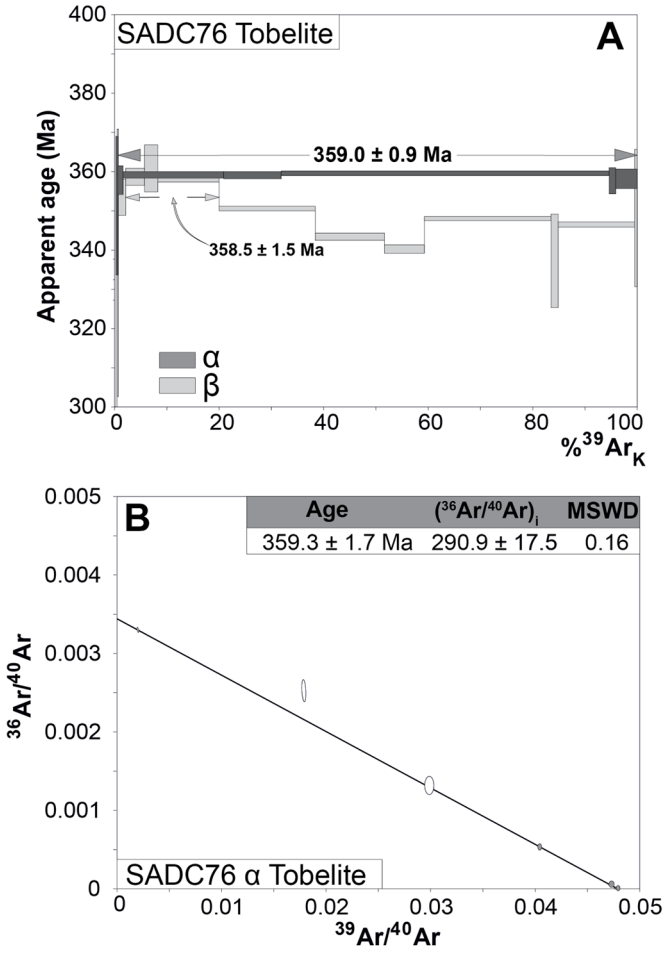

Fig. 5. A. Single grain $^{40}Ar/^{39}Ar$ dating of tobelite (from SADC76 sample) from vein of the hydrothermal stage 3 (Pb-Sb-Au). The age error bars for each temperature steps and plateau age are given at the 1 σ level. B. Inverse isochron analysis of the SADC76 α tobelite experiment.

4a, 4b) or crystals that grew between the vein wall and the quartz (Figs. 3d and 4c, 4d). Tobelite crystals from the SADC76 sample were analysed using Cameca SX50 electron probe micro-analysers (BRGM-CNRS-Orleans University). Compositions of tobelite and the analytical conditions are provided in Electronic Supplementary Materials 1 (ESM1). Figure 4e shows that radiating tobelite crystals from the core of the vein are slightly distinct from the tobelite grains located at the selvage of the quartz vein. These grains are indeed more enriched in K_2O than the tobelite crystals from the core (*i.e.* depleted in NH^+_4 and with a chemical evolution towards the NH^+_4-muscovite trend).

4 $^{40}Ar/^{39}Ar$ and U-Pb Geochronology

4.1 Tobelite $^{40}Ar/^{39}Ar$ dating

Tobelite crystals are only found within the quartz veins belonging to stage 3 in association with gold and antimony (Figs. 3a and 3b, Gloaguen *et al.*, 2007). Tobelite aggregates were thus selected for $^{40}Ar/^{39}Ar$ dating. They were carefully handpicked under a binocular microscope from the 0.25–1.0 mm fractions and analysed by $^{40}Ar/^{39}Ar$ step-heating with a CO_2 laser probe, following the analytical procedure described in Ruffet *et al.* (1991, 1995). Details on the method, calculation parameters and analytical data are given in ESM2.

Duplicated tobelite experiments (α and β) yielded two distinct but consistent age spectra. Experiment α displayed a plateau age (*ca.* 99.4% of $^{39}Ar_K$ released) at 359.0 ± 0.9 Ma (1 σ); whereas duplicate experiment β provided a saddle-shaped age spectrum (Fig. 5a). The inverse isochron analysis of experiment α (Fig. 5b; Turner, 1971; Roddick *et al.*, 1980; Hanes *et al.*, 1985), with a calculated $^{40}Ar/^{39}Ar$ initial ratio compliant with atmospheric one, rules out the possibility of excess argon s.s. and seemingly supports previous plateau age calculation. Nevertheless, it must be kept in mind that inverse isochron analysis does not allow detecting inherited argon, as shown by Ruffet *et al.* (1995) for a biotite (High Pressure tectonic context), and that such contamination is compatible with achievement of flat age spectra for biotite (*e.g.* Pankhurst *et al.*, 1973; Roddick *et al.*, 1980; Dallmeyer and Rivers, 1983; Foland, 1983) or phengite in HP context (*e.g.* Ruffet *et al.*, 1995, 1997). On the other hand, such behavior has never been documented for white micas out of the HP context.

Furthermore, the duplicate experiment β intrinsically substantiates the previously calculated *ca.* 359 Ma age. As a matter of fact, the saddle shape yielded by experiment β probably expresses the mixing of two tobelite components coming from the partial recrystallization of a primary tobelite crystals during a subsequent disturbing event (Cheilletz *et al.*, 1999; Alexandrov *et al.*, 2002; Castonguay *et al.*, 2007; Tartèse *et al.*, 2011; Tremblay *et al.*, 2011). According to the interpretation proposed by Alexandrov *et al.* (2002), saddle sidewalls apparent ages yield a minimum estimate of the primary component age, in this case, at least *ca.* 358.5 ± 1.5 Ma according to low to intermediate temperature steps. This apparent age is consistent with the plateau age obtained from experiment α and suggests that part of the primary tobelite was preserved during this recrystallization event and its radiogenic signal was fully isolated during degassing. However, this may not hold for the component that crystallized during the disturbing event. Referring back to the model proposed by Alexandrov *et al.* (2002) and according to the degree of separation achieved during degassing experiment, the apparent age of the base of the saddle (*ca.* 340 Ma in the present case) would represent a maximum age estimate for the secondary component, more or less close to the age of the subsequent disturbing event. The difference between the two experiments might be explained by the fact that the tobelite α was more enclosed (*i.e.* preserved) inside the quartz than the tobelite β (Figs. 3d and 4a, 4d), and consequently less sensitive to subsequent disturbing fluid flows. Indeed, EPMA analyses show a slight difference in the composition of the tobelite crystals from the border of the quartz vein (Fig. 4e). This could be related to fluid-tobelite interactions (*e.g.* more important at the border as evidenced by chlorite) as suggested by the following reaction (Pöter *et al.*, 2004): Tobelite + KCl (fluid) = Muscovite + NH4Cl (fluid). The partition coefficient of NH^+_4 indicates that fluids incorporate NH^+_4 more easily than tobelite (Pöter *et al.*, 2004). Fluids are able to exchange NH^+_4 and K gradually replacing tobelite in NH^+_4-rich muscovite and partially resetting the chronometer.

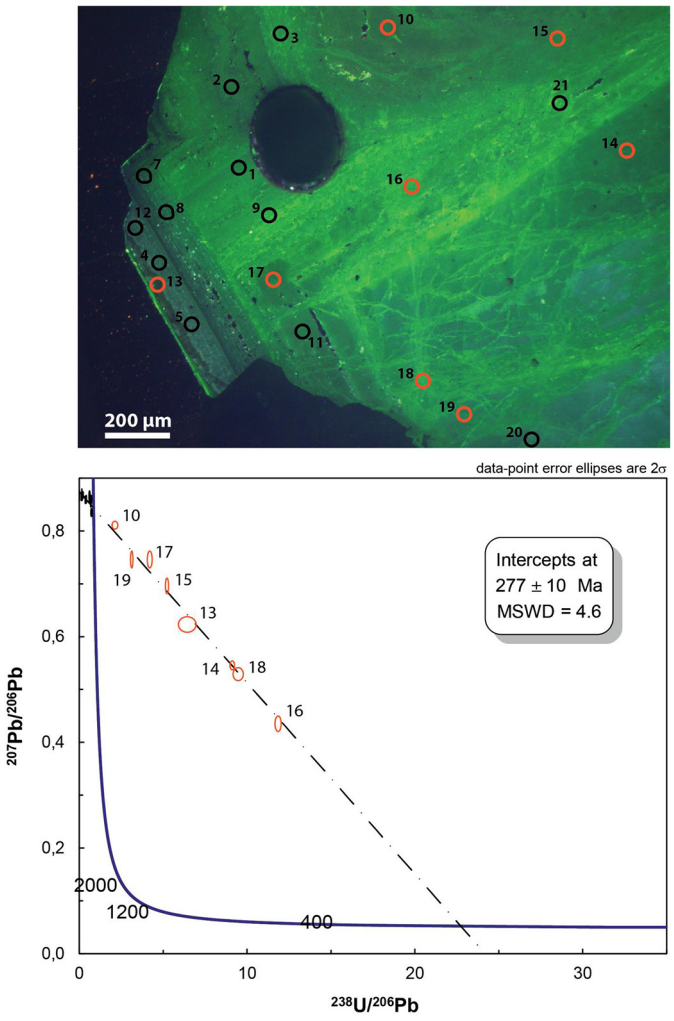

Fig. 6. A. CL image of a large fluoroapatite IV crystal from SADC (cold cathode type CITL Mk 5**,** 15 kV, 500 µA, defocalized beam of 4 mm diameter, 20° incidence angle, Mons Polytechnique University, Belgium). The black circle is cylindrical hollow formed by laser ablation performed in Moëlo *et al.* (2008). The growth banding is due to Sr (green) ↔ Ca (blue) substitution. Labelled laser spots correspond to U-Pb analyses reported in ESM2 (analysis No. 6 failed, whereas No. 22 and 23 are outside the photo framework). Labeled red circles correspond to analyses with radiogenic lead. B. Tera-Wasserburg diagram and intercept age obtained on fluorapatite IV from SADC.

We thus assume that tobelite would have initially crystallized at (or slightly before) *ca.* 359 Ma, which would be a minimum estimate for the age of the hydrothermal fluid flow responsible for the deposition of gold and antimony. Results further suggest that tobelite was partly recrystallized during a subsequent event at or younger than *ca.* 340 Ma.

4.2 Apatite U-Pb dating

Four generations of fluorapatite (hereafter named I to IV from older to younger, Moëlo *et al.*, 2008) have been described in the paragenetic sequence of the SADC mineralization: (1) the fluorapatite I resulted from recrystallization processes during a diagenetic/metamorphic event, (2) the fluorapatite II crystallized during the epigenetic massive sulphidation of OIH (stage 1), and (3) the fluorapatite III and IV post-dated this main sulphidation stage within OIH and crystallized at lower temperature conditions (Moëlo *et al.*, 2008). Fluorapatite IV formed from the dissolution of fluorapatite I and appears as euhedral zoned crystals within OIH cavities. Furthermore, neither mineralogical nor textural relationships allowed us to establish the precise timing of these last apatite generations with respect to the Sb ± Au stage 3. LA-ICP-MS U-Pb analytical procedure followed the method described in Pochon *et al.* (2016b). Details and standards analyses are given in ESM3. All errors are provided at 2 σ level.

Attempts to date the first three generations of apatite were unsuccessful because of the absence (or quasi absence) of uranium. Only the large fluorapatite IV crystal (Fig. 6a) studied by Moëlo *et al.* (2008) returned meaningful data. Plotted in a Tera-Wasserburg diagram (Fig. 6b), all data are discordant to very discordant.

A first group of analyses returned data that are almost radiogenic Pb free (black ellipses in Fig. 4b). A second group yielded less discordant data (red ellipses in Fig. 6b) allowing to draw a discordia, which returns a lower intercept date of 277 ± 10 Ma (MSWD = 4.6) and an initial $^{207}Pb/^{206}Pb$ value of *ca.* 0.86 compatible with the common Pb value given by the Stacey & Kramers (1975) Pb evolution model. Both groups of analyses are randomly distributed with respect to the Sr ↔ Ca substitution within growth bands and sealed micro-cracks (Fig. 6a and compared with electron microprobe mapping in Moëlo *et al.*, 2008). Therefore, despite of the erratic distribution of radiogenic Pb across the crystal, the fluorapatite IV within the OIH recorded an Early Permian event. These data also show that uranium was available in the fluids only during the Early Permian. Another explanation could be that all the available uranium was captured by xenotime and/or pretulite during the older fluid flow events, thus depleting the former apatite generations in uranium.

5 Discussion

5.1 Timing of Sb ± Au deposition in the Central Armorican Domain

The oldest $^{40}Ar/^{39}Ar$ plateau date measured at 359.0 ± 0.9 Ma (Fig. 4a) is interpreted as the crystallization age of tobelite. Because tobelite growth was contemporaneous with the deposition of Sb-sulfosalts and gold (Figs. 3a and 3b, Gloaguen *et al.*, 2007), this age also corresponds to the Sb ± Au mineralizing event (stage 3). Moreover, the temperature of the fluid responsible for this mineralizing event is estimated at around 275 °C (Gloaguen *et al.*, 2007). Assuming a closing temperature for tobelite, similar to that of white micas (around 300 °C), this $^{40}Ar/^{39}Ar$ plateau age, is likely not a cooling age. The oldest apparent age of the disturbed saddle-shaped spectrum, around 358 Ma (Fig. 5a), also strengthens this interpretation. As the Sb ± Au hydrothermal stage 3 is unequivocally the last metal-bearing mineralizing event at SADC (Gloaguen *et al.*, 2007), the massive sulphidation and base-metal stages (1 and 2) are older than 359 Ma, in contrast

to the former interpretation of Gloaguen *et al.* (2007) solely based on extensional veins analysis.

The age obtained on tobelite, coupled with the Late Devonian-Early Carboniferous ages recently obtained for the Le Semnon Sb ± Au mineralization (Fig. 1b, Pochon *et al.*, 2018), argues for a regional Sb ± Au mineralizing event that occurred around 360 Ma in the CAD. Therefore, we evidence an early mineralizing Sb ± Au event that predates the Late Carboniferous hydrothermal mineralizing event assumed for the CAD (Chauris & Marcoux, 1994; Bouchot *et al.*, 1997, 2005). However, a small-scale Sb occurrence described in Scubériou crosscuts the Visean sedimentary rocks in the Châteaulin basin (Fig. 1a). This indicates that another Sb mineralization event took place after 360 Ma. Although it is not the purpose of this study, it would be interesting to better characterize these distinct Sb ± Au events in the Armorican Massif.

Although the mineralizing event is relatively well dated around 360 Ma for SADC, there is geochronological evidence for subsequent hydrothermal activity. Indeed, the saddle-shape $^{40}Ar/^{39}Ar$ spectrum of tobelite β (Fig. 5a) indicates a partial re-equilibration of the isotopic system after 360 Ma (at a maximum age around 340 Ma). Such disturbance of the $^{40}Ar/^{39}Ar$ spectrum is also identified for illites from the Le Semnon Sb ± Au deposit (Pochon *et al.*, 2018). Furthermore, Tartèse *et al.* (2015) have shown that the U-Pb system of xenotime from the OIH were disturbed by one or several hydrothermal events, one of them occurring around of 340–330 Ma. Finally, our U-Pb data on the fluoroapatite IV from the OIH (Fig. 6b) indicates that an Early Permian fluid flow (*ca.* 280 Ma) was responsible for a (re-) crystallization of apatite. This last event could be in relation with the well-documented continental Early Permian hydrothermal events associated with the formation of numerous uranium deposits within the Armorican Massif (Ballouard *et al.*, 2017, 2018a and Fig. 1b).

Thus, the hydrothermal history of the SADC quarry appears to be polyphased with successive and discontinuous fluid pulses. At SADC, the last hydrothermal Permian event did not induce any significant remobilization or new deposition of metals.

5.2 Depth and hydrodynamics of the Sb ± Au deposition in the Central Armorican Domain

At SADC, the Sb ± Au mineralization is hosted by the early Ordovician Armorican Quartzite. At 360 Ma, the sedimentary thickness overlying the Sb ± Au active hydrothermal system cannot have exceeded 2800 meters at SADC (*i.e.* around 72 MPa without a potential free water column, see Pochon *et al.*, 2018 for further details). This constraint implies a shallow depth for the metal deposition. Considering an elevated geothermal gradient of 50 °C/km, a maximum temperature of around 140 °C can be estimated for the Ordovician rock hosting mineralization at SADC. With respect to the temperature estimate for the mineralizing stage (300–275 °C; Gloaguen *et al.*, 2007), it appears that the mineralizing fluids may have been in a strong thermal disequilibrium with the host rocks. Therefore, a hot advective upward fluid flow is required. Similar shallow formation depth and advective regime are also recognized for the Le Semnon Sb ± Au ore deposit (Pochon *et al.*, 2018). In this hydrothermal context, the N160°E-trending faults of the CAD (Fig. 1a) probably acted as high permeability zones enhancing advective mineralizing fluid flows. By inference, most of these N160°E-trending faults (*e.g.* at SADC, Figs. 2a, 2b) were already active during the Early Carboniferous. These structures may well have been active subsequently during the Variscan history, localizing the hydrothermal fluids up to Permian times.

5.3 Tectonic, magmatic and metallogenesis regional framework

At 360 Ma, the CAD was an unthickened incipient fold belt subjected to the initiation of a regional-scale simple shear (Gumiaux *et al.*, 2004). At a larger scale, this incipient CAD fold belt was in supra-continental subduction context, as demonstrated by the early Carboniferous ages of high-pressure/low-temperature metamorphism peak recorded in the South Armorican Variscan internal domain, which was associated with northward-dipping subduction of the North Gondwana margin (Bosse *et al.*, 2000, 2005; Ballèvre *et al.*, 2014; Gapais *et al.*, 2015). In detail, this period corresponds to a plate dynamic shift from Gondwana-Armorica continental subduction to collision with subsequent Middle-Late Carboniferous nappe stacking and exhumation in the internal domains. This tectonic shift temporarily coincides with the large-scale mafic magmatism spreading over the Central and North Armorican external domains (Fig. 1a; Pochon *et al.*, 2016b). Plate-scale boundary conditions are not yet clearly established, but the coeval occurrence of a HP-LT metamorphic event that produced eclogites in the internal part of the belt, to the south of the suture zone, and the widespread development of a mafic magmatism in the upper plate is noteworthy. Further investigations are necessary to understand this first-order observation.

Within Carboniferous basins, Late Devonian-Early Carboniferous volcanism was responsible for a major metallogenic event, leading to base metal volcanogenic massive sulphides (VMS) deposition, located in the Devono-Carboniferous basins at the scale of the whole Variscan belt (Lescuyer *et al.*, 1997 and Fig. 1b). Although there is no apparent genetic relationships between Sb ± Au mineralization and base metal VMS through the Armorican Massif, it could be interesting to investigate potential relationships between these two events, because Lescuyer *et al.* (1997) did not evaluate the extent of the magmatism (responsible for VMS deposits) outside the basins. Based on our data and the recent works of Pochon *et al.* (2016a, b, 2018), we infer that this mafic magmatism and the related thermal anomaly might have affected the external whole domains of the belt around 360 Ma. Indeed, the Central Iberian Zone (*i.e.* the CAD counterpart in the Iberian Massif) hosts the twin deposit of SADC (Gloaguen *et al.*, 2016) as well as numerous similar Sb ± Au deposits and various mafic magmatic bodies (*e.g.* Couto *et al.*, 1990). This *ca.* 360 Ma magmatic event has locally triggered hydrothermal fluid flow favourable for Sb ± Au mineralization, probably by expelling fluids from the surroundings rocks. This might have important consequence for exploration strategy throughout the Variscan belt.

6 Conclusions

New $^{40}Ar/^{39}Ar$ and U-Pb dating of tobelite and apatite from the Saint-Aubin-des-Châteaux base metal-Sb ± Au occurrence allow us to underline the following points:

- the Sb ± Au deposition is Late Devonian – Early Carboniferous in age. Coupled with recent results obtained on the Le Semnon northernmost Sb ± Au district, a 360 Ma old economic Sb ± Au mineralizing peak is identified in the southeastern part of the Central Armorican Domain;
- post-dating this *ca.* 360 Ma Sb ± Au mineralizing peak, absolute dating of fluorapatite allows identifying a subordinate Early Permian hydrothermal event. This late alteration did not induce any significant metal deposition or remobilization at SADC;
- the Sb ± Au mineralizing hydrothermal event coincides with a widespread mafic magmatism, which can be considered as a major trigger for the mineralizing systems and a major heat source for the initiation of hot advective fluid flows at shallow depths (less than 3 km). This Early Carboniferous mafic magmatism has to be (re-) considered in mineralizing system genesis studies within the Variscan belt. In particular, the potential relationships between the Variscan Sb ± Au deposits and the base metal volcanogenic massive sulfides deposits in Devono-Carboniferous basins should be further explored;
- first dating of tobelite crystals show that this mineral can be used to date gold deposits hosted in carbonaceous matter-rich rocks using the $^{39}Ar/^{40}Ar$ method.

Acknowledgements. We are very grateful to Yves Moëlo who provided us the "historical" polished section of apatite grains from the Saint-Aubin-des-Châteaux deposit. We also thank Sylvain Janiec and Xavier Le Coz for thin section preparation. F. Grasset and C. Friot from the HERVE SA group have greatly facilitated access to the Saint-Aubin-des-Châteaux quarry. This study has been granted by INSU through the CESSUR Project 2016 (Coord. M. Poujol), the BRGM and the Région Bretagne. We gratefully thank the editors L. Jolivet and R. Augier who helped to greatly improve the manuscript as well as three anonymous reviewers for their constructive comments.

References

Alexandrov P, Ruffet G, Cheilletz A. 2002. Muscovite recrystallization and saddle-shaped $^{40}Ar/^{39}Ar$ age spectra: Example from the Blond granite (Massif Central, France). *Geochim Cosmochim Ac* 66: 1793–1807.

Augier R, Choulet F, Faure M, Turrillot P. 2015. A turning-point in the evolution of the Variscan orogen: The *ca.* 325 Ma regional partial-melting event of the coastal South Armorican domain (South Brittany and Vendée, France). *Bull Soc géol Fr* 186: 63–91.

Ballèvre M, Catalán JRM, López-Carmona A, Pitra P, Abati J, Fernández RD, *et al.* 2014. Correlation of the nappe stack in the Ibero-Armorican arc across the Bay of Biscay: A joint French-Spanish project. *Geol Soc Spec Publ* 405: 77–113.

Ballouard C, Poujol M, Boulvais P, Mercadier J, Tartèse R, Venneman T, *et al.* 2017. Magmatic and hydrothermal behavior of uranium in syntectonic leucogranites: The uranium mineralization associated with the Hercynian Guérande granite (Armorican Massif, France), *Ore Geol Rev* 80: 309–331.

Ballouard C, Poujol M, Mercadier J, Deloule E, Boulvais P, Baele JM, *et al.* 2018a. Uranium metallogenesis of the peraluminous leucogranite from the Pontivy-Rostrenen magmatic complex (French Armorican Variscan belt): The result of long-term oxidized hydrothermal alteration during strike-slip deformation. *Miner Deposita* 53: 601–628.

Ballouard C, Poujol M, Zeh A. 2018b. Multiple crust reworking in the French Armorican Variscan belt: Implication for the genesis of uranium-fertile leucogranites. *Int J Earth Sci* 107: 2317–2336.

Bentabol M, Cruz MDR. 2016. Characterization of tobelite formed from kaolinite under hydrothermal conditions (200 °C). *Appl Clay Sci* 126: 160–172.

Bosse V, Féraud G, Ruffet G, Ballèvre M, Peucat J-J, De Jong K. 2000. Late Devonian subduction and early-orogenic exhumation of eclogite-facies rocks from the Champtoceaux Complex (Variscan belt, France). *Geol J* 35: 297–325.

Bosse V, Féraud G, Ballèvre M, Peucat J-J, Corsini M. 2005. Rb-Sr and 40Ar/39Ar ages in blueschists from the Ile de Groix (Armorican Massif, France): Implications for closure mechanisms in isotopic systems. *Chem Geol* 220: 21–45.

Bouchot V, Milesi JP, Lescuyer JL, Ledru P. 1997. Les minéralisation aurifères de la France dans leur cadre géologique autour de 300 Ma. *Chron Rech Min* 528: 13–62.

Bouchot V, Ledru P, Lerouge C, Lescuyer JL, Milesi JP. 2005. 5: Late Variscan mineralizing systems related to orogenic processes: The French Massif Central. *Ore Geol Rev* 27: 169–197.

Capdevila R. 2010. Les granites varisques du Massif Armoricain. *B Soc Géol Min Br Série* D(7): 1–52.

Capitani GC, Schingaro E, Lacalamita M, Mesto E, Scordari F. 2016. Structural anomalies in tobelite-2M2 explained by high resolution and analytical electron microscopy. *Mineral Mag* 80: 143–156.

Castonguay S, Ruffet G, Tremblay A. 2007. Dating polyphase deformation across low-grade metamorphic belts: An example based on $^{40}Ar/^{39}Ar$ muscovite age constraints from the southern Quebec Appalachians, Canada. *Geol Soc Am Bull* 119: 978–992.

Charonnat X. 2000. Les minéralisations aurifères tardi-hercyniennes des Cévennes, Unpublished PhD thesis: University of Orléans, 259 p.

Chauris L, Houlgatte E, Laforêt C, Picot P. 1985. Un district antimono-aurifère à gangue quartzo-carbonatée: Le Semnon (Ille-et-Vilaine, Massif Armoricain, France). *Hercynica* 1: 111–119.

Chauris L, Marcoux E. 1994. Metallogeny of the Armorican Massif. In: Chantraine J, Rolet J, Santallier DS, *et al.,* eds. Pre-Mesozoic geology in France and related areas. Springer Berlin Heidelberg, pp. 243–264.

Chauvel JJ. 1974. Les minerais de fer de l'Ordovicien inférieur du bassin de Bretagne-Anjou, France. *Sedimentology* 21: 127–147.

Chauvet A, Volland-Tuduri N, Lerouge C, Bouchot V, Monié P, Charonnat X, *et al.* 2012. Geochronological and geochemical characterization of magmatic-hydrothermal events within the southern Variscan external domain (Cévennes Area, France). *Int J Earth Sci* 101: 69–86.

Cheilletz A, Ruffet G, Marignac C, Kolli O, Gasquet D, Féraud G, *et al.* 1999. $^{40}Ar/^{39}Ar$ dating of shear zones in theVariscan basement of Greater Kabilia (Algeria). Evidence of an Eo-Alpine event at 128 Ma (Hauterivian-Barremian boundary): Geodynamic consequences. *Tectonophysics* 306: 97–116.

Choukroune P, Lopez-Munoz M, Ouali J. 1983. Cisaillement ductile sud-armoricain et déformations discontinues associées: mise en évidence de la déformation régionale non coaxiale dextre. *C R Acad Sci Paris* 296: 657–660.

Couto H, Roger G, Moëlo Y, Bril H. 1990. Le district à antimoine-or Dúrico-Beirão (Portugal): évolution paragénétique et géochimique; implications métallogéniques. *Miner Deposita* 25(1): S69–S81.

Costa S, Rey P. 1995. Lower crustal rejuvenation and growth during post-thickening collapse: Insights from a crustal cross section through a Variscan core complex. *Geology* 23: 905–908.

Dallmeyer RD, Rivers T. 1983. Recognition of extraneous argon components through incremental-release $^{40}Ar/^{39}Ar$ analysis of biotite and hornblende across the Grenvillian metamorphic gradient in southwestern Labrador. *Geochim Cosmochim Ac* 47: 413–428.

Foland KA. 1983. $^{40}Ar/^{39}Ar$ incremental heating plateaus for biotites with excess argon. *Chem Geol* 1: 3–21.

Frost RL, López A, Belotti FM, Xi Y, Scholz R. 2014. A vibrational spectroscopic study of the phosphate mineral lulzacite $Sr_2Fe^{2+}(Fe^{2+},Mg)_2Al_4(PO_4)_4(OH)_{10}$. *Spectrochim Acta A* 127: 243–247.

Gapais D, Le Corre C. 1980. Is the Hercynian belt of Brittany a major shear zone? *Nature* 288: 574–576.

Gapais D, Brun J.P, Gumiaux C, Cagnard F, Ruffet G, Le Carlier de Veslud C. 2015. Extensional tectonics in the Hercynian Armorican belt (France). An overview. *Bull Soc géol Fr* 186 (2–3): 117–129.

Gloaguen E, Branquet Y, Boulvais P, Moelo Y, Chauvel J-J, Chiappero P-J, *et al*. 2007. Palaeozoic oolitic ironstone of the French Armorican Massif: A chemical and structural trap for orogenic base metal–As–Sb–Au mineralization during Hercynian strike-slip deformation. *Miner Deposita* 42: 399–422.

Gloaguen E, Branquet Y, Urien P, Boulvais P, Poujol M, Tartèse R. 2016. How much hidden oolitic iron ore-hosted precious and base metals deposits should be encountered in the Variscan belt? Insights from France and Portugal. 25ème Réunion des Sciences de la Terre – Earth Sciences meeting, 24–28 octobre 2016, Caen, France. Abstract volume, p. 141.

Gumiaux C, Gapais D, Brun JP, Chantraine J, Ruffet G. 2004. Tectonic history of the Hercynian Armorican Shear belt (Brittany, France). *Geodin Acta* 17: 289–307.

Hanes JA, York D, Hall CM. 1985. An $^{40}Ar/^{39}Ar$ geochronological and electron microprobe investigation of an Archean pyroxenite and its bearing on ancient atmospheric compositions. *Can J Earth Sci* 22: 947–958.

Hall CM, Higueras PL, Kesler SE, Lunar R, Dong H, Halliday AN. 1997. Dating of alteration episodes related to mercury mineralization in the Almadén district, Spain. *Earth Plant Sci Lett* 148: 287–298.

Le Corre C. 1978. Approche quantitative des processus synschisteux. L'exemple du segment Hercynien de Bretagne Centrale. Unpubl. Doctoral dissertation, Rennes: Université de Rennes 1, 382 p.

Léone P, Palvadeau P, Moëlo Y. 2000. Structure cristalline d'un nouveau phosphate de strontium naturel (lulzacite), $Sr_2Fe^{2+}(Fe^{2+},Mg)_2Al_4(PO_4)_4(OH)_{10}$. *C R Acad Sci Paris* IIc(3): 301–308.

Lescuyer JL, Leistel JM, Marcoux E, Milési JP, Thiéblemont D. 1997. Late Devonian-Early Carboniferous peak sulphide mineralization in the Western Hercynides. *Miner Deposita* 33: 208–220.

Marcoux E, Fouquet Y. 1980. Âge des filons plombo-zincifères du Cap Sizun. Apport de la géochronologie. Abstract, Réun. ann. Se. Terre. Marseille 1980.

Marcoux E, Serment R, Allon A. 1984. Les gîtes d'antimoine de Vendée (Massif Armoricain, France). Historique des recherches et synthèse métallogénique. *Chron Rech Min* 476: 3–30.

Mesto E, Scordari F, Lacalamita M, Schingaro E. 2012. Tobelite and NH^{4+}-rich muscovite single crystals from Ordovician Armorican sandstones (Brittany, France): Structure and crystal chemistry. *Am Mineral* 97: 1460–1468.

Moëlo Y, Lasnier B, Palvadeau P, Léone P, Fontan F. 2000. La Lulzacite, $Sr_2Fe^{2+}(Fe^{2+},Mg)_2Al_4(PO_4)_4(OH)_{10}$, un nouveau phosphate destrontium (Saint-Aubin-Des-Chateâux, Loire-Atlantique, France). *C R Acad Sci Paris* 330: 314–324.

Moëlo Y, Lulzac Y, Rouer O, Palvadeau P, Gloaguen E, Léone P. 2002. Scandium mineralogy: Pretulite with scandian zircon and xenotime-(Y) within an apatite-rich oolitic ironstone from Saint-Aubin-Des-Châteaux, Armorican Massif, France. *Can Miner* 40: 1657–1673.

Moëlo Y, Rouer O, Bouhnik-Le Coz M. 2008. From diagenesis to hydrothermal recrystallisation: Polygenic Sr-rich fluorapatite from the oolitic ironstone of Saint-Aubin-des-Châteaux (Armorican Massif, France). *Eur J Mineral* 20: 205–216.

Neiva AMR, Andráš P, Ramos JMF. 2008. Antimony quartz and antimony-Gold quartz veins from northern Portugal. *Ore Geol Rev* 34: 533–546.

Pankhurst RJ, Moorbath S, Rex DC, Turner G. 1973. Mineral age patterns in *ca.* 3700 my old rocks from West Greenland. *Earth Planet Sci Lett* 20: 157–170.

Pierrot R, Chauris L, Laforet C. 1975. Inventaire minéralogique de la France (Côtes-du-Nord), 5. Orléans: BRGM, 220 p.

Pochon A, Gapais D, Gloaguen E, Gumiaux C, Branquet Y, Cagnard F, *et al.* 2016a. Antimony deposits in the Variscan Armorican belt, a link with mafic intrusives? *Terra Nova* 28: 138–145.

Pochon A, Poujol M, Gloaguen E, Branquet Y, Cagnard F, Gumiaux C, *et al.* 2016b. U-Pb LA-ICP-MS dating of apatite in mafic rocks: Evidence for a major magmatic event at the Devonian-Carboniferous boundary in the Armorican Massif (France). *Am Mineral* 101: 2430–2442.

Pochon A, Beaudoin G, Branquet Y, Boulvais P, Gloaguen E, Gapais D. 2017. Metal mobility during hydrothermal breakdown of Fe-Ti oxides: Insights from Sb-Au mineralizing event (Variscan Armorican Massif, France). *Ore Geol Rev* 91: 66–99.

Pochon A, Gloaguen E, Branquet Y, Poujol M, Ruffet G, Boiron MC, *et al.* 2018. Variscan Sb-Au mineralization in central Brittany (France): A new metallogenic model derived from the Le Semnon district. *Ore Geol Rev* 97: 109–142.

Pöter B, Gottschalk M, Heinrich W. 2004. Experimental determination of the ammonium partitioning among muscovite, K-feldspar, and aqueous chloride solutions. *Lithos* 74: 67–90.

Roddick JC, Cliff RA, Rex DC. 1980. The evolution of excess argon in Alpine biotites – A $^{40}Ar/^{39}Ar$ analysis. *Earth Planet Sci Lett* 48: 185–208.

Ruffet G, Féraud G, Amouric M. 1991. Comparison of $^{40}Ar/^{39}Ar$ conventional and laser dating of biotites from the North Tregor batholith. *Geochim Cosmochim Ac* 55: 1675–1688.

Ruffet G, Féraud G, Ballèvre M, Kiénast JR. 1995. Plateau ages and excess argon in phengites: A ^{40}Ar-^{39}Ar laser probe study of Alpine micas (Sesia Zone, Western Alps, northern Italy). *Chem Geol (Isotopic Geoscience Section)* 121: 327–343.

Ruffet G, Gruau G, Ballèvre M, Féraud G, Philippot P. 1997. Rb-Sr and ^{40}Ar-^{39}Ar laser probe dating of high-pressure phengites from the Sesia zone (Western Alps): Underscoring of excess argon and new age constraints on the high-pressure metamorphism. *Chem Geol* 141: 1–18.

Stacey JS, Kramers JD. 1975. Approximation of terrestrial lead isotope evolution by a two-stage model. *Earth Planet Sci Lett* 26: 207–221.

Tartèse R, Ruffet G, Poujol M, Boulvais P, Ireland TR. 2011. Simultaneous resetting of the muscovite K-Ar and monazite U-Pbgeochronometers: A story of fluids. *Terra Nova* 23: 390–398.

Tartèse R, Poujol M, Gloaguen E, Boulvais P, Drost K, Košler J, *et al.* 2015. Hydrothermal activity during tectonic building of the

Variscan orogen recorded by U-Pb systematics of xenotime in the GrèsArmoricain formation, Massif Armoricain, France. *Miner Petrol* 109: 485–500.

Tremblay A, Ruffet G, Bédard JH. 2011. Obduction of Tethyan-type ophiolites – A case-study from the Thetford-Mines ophiolitic Complex, Quebec Appalachians, Canada. *Lithos* 125: 10–26.

Turner, G. 1971. Argon 40-argon 39 dating: The optimization of irradiation parameters. *Earth Planet Sci Lett* 10: 227–234.

Vernhet Y, Plaine J, Trautmann F, Pivette B. 2009. Geological map of France (1/50 000), notice of the Cossé-le-Vivien sheet (355), Orléans, France: BRGM, 222 p.

Wilson PN, Parry WT, Nash WP. 1992. Characterization of hydrothermal tobelitic veins from black shale, Oquirrh Mountains, Utah. *Clay Clay Miner* 40: 405–420.

Yesares L, Sáez R, Nieto JM, De Almodovar GR, Gómez C, *et al*. 2015. The Las Cruces deposit, Iberian Pyrite Belt, Spain. *Ore Geol Rev* 66: 25–46.

Cite this article as: Pochon A, Branquet Y, Gloaguen E, Ruffet G, Poujol M, Boulvais P, Gumiaux C, Cagnard F, Baele J-M, Kéré I, Gapais D. 2019. A Sb ± Au mineralizing peak at 360 Ma in the Variscan belt, *BSGF - Earth Sciences Bulletin* 190: 4.